Build Simul (2019) 12: 465–473
https://doi.org/10.1007/s12273-018-0497-x

A numerical investigation on the mixing factor and particle deposition velocity for enclosed spaces under natural ventilation

Xiaoran Liu[1], Fei Li[1] (✉), Hao Cai[1], Bin Zhou[1], Shanshan Shi[2], Jinxiang Liu[1]

1. Department of HVAC, College of Urban Construction, Nanjing Tech University, Nanjing 210009, China
2. School of Architecture and Urban Planning, Nanjing University, Nanjing 210007, China

Abstract

The multi-zone model is widely used to predict airflow and contaminant transport in large buildings under natural or mechanical ventilation. Selecting appropriate mixing factors and particle deposition velocities for the multi-zone model can compensate for the errors resulting from the model's well-mixing assumption. However, different room types, air change rates and ventilation modes can result in different mixing factors and particle deposition velocities. This study selected three typical room types: Z-type, L-type, and rectangle type (R-type). For each room type, the mixing factors and particle deposition velocities were investigated by the CFD model under different natural ventilation rates (0.5 h^{-1}, 1 h^{-1}, 3 h^{-1}, 6 h^{-1}, 12 h^{-1} and 20 h^{-1}) and modes (door-inlet, window-inlet). The results showed that the mixing factor of the Z-type room was the highest, and the mixing factors of these rooms were 1.32, 1.28 and 1.13, respectively. In addition, the mixing factors presented a V-shaped distribution as a function of the air exchange rate under the window-inlet mode. The particle deposition velocity increased as the air change rate increased, and also demonstrated that the V-shaped curves as a function of particle size (0.05 μm, 0.1 μm, 0.5 μm, 1 μm, 2.5 μm, 5 μm) varied under different air change rates and room types. The results of mixing factors and particle deposition velocities for different room types, air change rates and ventilation modes can be used to improve the accuracy of the multi-zone model.

Keywords

mixing factor,
particle deposition velocity,
computational fluid dynamics (CFD),
multi-zone model

Article History

Received: 3 August 2018
Revised: 28 October 2018
Accepted: 12 November 2018

1 Introduction

Most people spend 85%–90% of their time indoors (Chen and Zhao 2011), so indoor air quality (IAQ) is important for people's health. It is meaningful to research the transport of contaminants in enclosed spaces for good air quality. There are many methods of calculating the contaminant dispersion in buildings, such as analytical models, empirical models, small-scale experimental models, full-scale experimental models, multi-zone models, zonal models, and computational fluid dynamics (CFD) models (Chen 2009). The multi-zone model represents buildings as networks of well-mixed zones that are connected with some discrete flow paths, such as ducts, doors and windows, and proceeds with a simultaneous solution for the mass balance equations of the zones. It is widely used for building airflow and contaminant transport simulation (Michaelides et al. 2014; Zhai and Jin 2018) due to its fast and effective computation (Axley 2007; Wang and Chen 2008a). However, the well-mixed assumption could cause errors for the simulation of airflow under special conditions, such as with strong buoyancy, large contaminant concentration gradient, or strong momentum (Wang and Chen 2008b). Gadgil et al. (2003) also reported that the well-mixed assumption is too simplistic. Therefore, it is necessary to study methods for improving the multi-zone model for its better application.

One improvement method is to integrate new solvers into the multi-zone model. Ndione et al. (2008) and Wang et al. (2010) presented a method of coupling multi-zone and CFD for building simulation, which can be used to predict airflow and contaminant distributions when the well-mixing assumption is not appropriate for the specific zone studied. Lorenzetti et al. (2013) presented a general-purpose code for ordinary differential equations, by which the new solver

E-mail: faylee@njtech.edu.cn

List of symbols

a	air exchange rate (s^{-1})	u^*	friction velocity (cm/s)
A	area of inner surface (m^2)	u	horizontal component of the mean velocity (m/s)
A_i	area of i-th boundary face (m^2)	U	mean velocity (m/s)
A_{inlet}	area of inlet (m^2)	v	vertical component of the mean velocity (m/s)
C	contaminant concentration of indoor air ($\mu g/m^3$)	v_d	deposition velocity (m/s)
C_0	initial contaminant concentration of indoor air ($\mu g/m^3$)	v_{di}	deposition velocity of i-th boundary face (m/s)
		V	room volume (m^3)
C_{out}	contaminant concentration of outdoor air ($\mu g/m^3$)	W	Okubo-Weiss parameter
d_p	particle diameter (μm)	β	particle deposition rate (s^{-1})
G	generation rate of internal sources ($\mu g/(m^3 \cdot s)$)	$\Gamma_{\Phi,eff}$	effective diffusion coefficient (m^2/s)
i	CFD cell index	ε	ratio of the opening area to the total area
I	turbulence intensity	ε_{inlet}	turbulence dissipation rate (m^2/s^3)
k	mixing factor	θ	inclination angle (°)
k_{inlet}	turbulence kinetic energy (m^2/s^2)	ρ	air density (kg/m^3)
n	total number of faces	τ	time constant (s)
Q	room supply ventilation rate (m^3/s)	τ_{exp}	time required for the breathing zone concentration to decay to 1/e of the initial concentration (s)
s_n	stretching deformation		
s_s	shearing deformation	Φ	variables
S_Φ	source term	ω	vorticity

could feature variable time steps, high-order integration methods, and automatic error controls. These can make the multi-zone model more accurate when simulating fast transport mechanisms, such as high air change rates and chemical reactions. Although these studies confirmed the complete mixing hypothesis resulted in some errors and proposed improvements for the multi-zone model, these improvements were based on more complex algorithms, such as CFD models and differential equations and cost more computation time.

Apart from integrating new solvers, selecting an appropriate "mixing factor" and deposition velocity for the particulate contaminant in the multi-zone model may be a better method because these two parameters can be used as adjustment factors in the mass balance equations of the multi-zone model directly and compensate for the well-mixing assumption (Zhong 2004). The "mixing factor" that represented the mixing degree in a room without fans (Drivas et al. 1972) was used to assess the effectiveness of a ventilation system by Kang and Chang (2005). Gadgil et al. (2003) reported that the mixing time is largely dependent on the room airflow pattern and partly on the source location. The selection of the mixing time for the pollutant transient transports under mechanical ventilation was also studied by Foat et al. (2017). Deng et al. (2017) employed a dimensionless time scale ratio and vorticity to investigate the influence of air change rates on indoor CO_2 stratification and removal. They found CO_2 stratification varied greatly with different air change rates and vent-inlet-sizes. All the research found that the influence of mixing time cannot be ignored for indoor contaminant transport studies.

For particle deposition velocity, Zhao et al. (2009) proposed an improved drift-flux model to analyse the particle deposition velocity under two different ventilation systems (mixing and displacement ventilation). Gao and Niu (2007) applied the drift-flux model to calculate the mean deposition velocity and human exposures to particles under mixing ventilation (MV), displacement ventilation (DV) and under floor air distribution system (UFAD), and their study revealed that the effects of the particle size, the ventilation type and the air exchange rate on the deposition rate cannot be neglected. He et al. (2005) investigated particle size distributions in 14 residential houses in Australia, and the results also showed that the measured particle deposition rates were size dependent and associated with large divisions between different houses. The relationship between natural ventilation rate and PM2.5 deposition rate/velocity in two university classrooms was examined in the study of Liu et al. (2018), and their experimental results showed that the PM2.5 deposition rate was positively associated with the natural ventilation rate. In summary, the important parameters in the mass balance model, such as the ventilation rate, particle deposition rate and mixing factor, have been investigated in previous studies. However, the interactive influences among these parameters (i.e., the influence of the room type, air change rate per hour (ACH) and ventilation

modes on the mixing time and particle deposition velocity) have not been fully considered.

This study aims to investigate the variations in the mixing factor and particle deposition velocity for enclosed spaces under different situations. These two parameters can be used as adjustment factors in the mass balance equations of the multi-zone model. We selected three typical room types: Z-type, L-type, and rectangle (R-type); and for each room type, we simulated the airflow fields under two natural ventilation modes by a validated CFD model. Based on the airflow fields, the mixing factors and particle deposition velocities for different particle sizes under different airflow situations were analysed.

2 Methodology

2.1 Definitions of the mixing factor and particle deposition velocity

The discussion on the effect of nonideal mixing of indoor air on pollutant attenuation was first reported by Lidwell and Lovelock (1946). The next discussion about the nonideal mixing appeared in an article by Brief (1960), in which the term of mixing factor was first coined. Afterwards, Constance (1970) discussed the air exchange required to remove contaminants from an enclosed air space. Subsequently, mixing factor as an index of characterizing the effectiveness of room ventilation was first measured in real experiment by Drivas et al. (1972). Assuming that a contaminant with an initial concentration of C_0 is released in a room with a volume of V and a ventilation rate of Q, under a well-mixed condition, according to mass balance, the following equation can be obtained:

$$V\frac{\mathrm{d}C}{\mathrm{d}t} = -CQ \tag{1}$$

The solution of Eq. (1) is:

$$C = C_0 \mathrm{e}^{(-Q/V)t} \tag{2}$$

where C is the indoor concentration, and t is the elapsed time. However, in reality, it takes some time to reach a complete mixing condition. In the ASHRAE standard, the breathing zone is defined as a region within an occupied space between planes 3 and 72 in. (75 and 1800 mm) above the floor and more than 2 ft (600 mm) from the walls or fixed air-conditioning equipment (ASHRAE 2004). The mixing factor was determined on the basis of the concentration difference between the breathing zone and the other regions. The formula for calculating the concentration with the mixing factor is given by the following (Drivas et al. 1972):

$$C = C_0 \mathrm{e}^{k(-Q/V)t} \tag{3}$$

where k is the mixing factor, it is the ratio of the time constant τ to the time, τ_{exp}, required for the breathing zone concentration to decay to 1/e of the initial concentration, and can be expressed as:

$$k = \frac{\tau}{\tau_{exp}} = \frac{V/Q}{\tau_{exp}} \tag{4}$$

The parameter of τ_{exp} can be obtained by measured data, and it also can be calculated through the user-defined scalar (UDS) in the simulation. Note that, Eqs. (1)–(4) do not work for particles, because the parameter τ should consider the effect of deposition. The mixing factor represents the mixing degree of fresh air and indoor air. A unit mixing factor means perfect mixing in the room. When the mixing factor is larger than one, it indicates a higher ventilation efficiency, and the ventilation pattern in the room is close to piston ventilation. In contrast, when the mixing factor is smaller than one, it means a lower ventilation efficiency, and the pollutant in the breathing zone is more difficult to exhaust.

The difference in particle deposition velocity under different scenarios is another research focus. You et al. (2012) developed empirical equations to calculate the particle deposition velocity on different angles of smooth planar surfaces with various particle diameters. Their equations can be divided into four parts: “fine zone”, “coarse zone”, “zero zone”, and “transition zone”. The specific equations for each scenario are as follows:

$$v_d = \begin{cases} (5.15\times10^{-8}u^* - 5.63 \times 10^{-11})d_p^{-1.263} & d_p < 0.0512(u^*)^{0.4227} \\ 3.7\times10^{-5}d_p^{1.9143}(\cos\theta) & d_p > 0.03577(\cos\theta)^{-0.41}, \cos\theta > 0 \\ 0 & d_p > g(u^*, \cos\theta), \cos\theta \le 0 \\ f(u^*, \cos\theta, d_p) & \text{for other} \end{cases} \tag{5}$$

where

$$\begin{aligned} \log[g(u^*,\cos\theta)] &= -0.941 + 0.796\log u^* + 0.333\cos\theta \\ &+ 0.1841\log u^*\cos\theta - 0.011(\log u^*)^2 + 0.15(\cos\theta)^2 \\ \log[f(u^*,\cos\theta,d_p)] &= -6.026 + 0.116\log u^* + 1.837\cos\theta \\ &+ 1.079\log d_p - 0.653\log u^*\cos\theta - 0.89\log u^*\times\log d_p \\ &+ 1.484\log d_p\cos\theta + 0.17(\log u^*)^2 - 0.074\cos^2\theta \\ &+ 1.076(\log d_p)^2 \end{aligned} \tag{6}$$

where u^* is the friction velocity, and d_p is the particle diameter. For the average deposition velocity, it can be calculated as (You et al. 2012):

$$v_{\mathrm{d}} = \frac{\sum_{i=1}^{n} v_{\mathrm{d}i} A_i}{\sum A_i} \tag{7}$$

where $v_{\mathrm{d}i}$ and A_i are the deposition velocity and area of i-th boundary face, and n is the total number of faces. The particle deposition rate can be obtained as:

$$\beta = v_{\mathrm{d}} \frac{A}{V} \tag{8}$$

where β is the particle deposition rate, and A is the inner surface area. The well-mixing assumption can be compensated by substituting the calculated results of mixing factor and deposition velocity into Eq. (9) as follows:

$$\frac{\mathrm{d}C}{\mathrm{d}t} = kaC_{\mathrm{out}} - (ka + \beta)C + G \tag{9}$$

where a is the air exchange rate, G is the generation rate of internal sources, and C_{out} is the pollutant concentration of outdoor air.

2.2 Case setup

In the study of Shi et al. (2015), 180 representative residences are used to investigate the annual and seasonal average infiltration rates in Beijing. Referring to their study, we selected three most common and typical room types: rectangle (R-type), Z-type, and L-type (Fig. 1). The yellow zones in the figure are breathing zones. The volumes of the rooms are 39 m^3, 42 m^3, and 56 m^3, respectively. The sizes of the window and door are 1.6 m × 1.6 m and 0.8 m × 2 m, and they determine the natural ventilation mode of the room. No heat source exists in the room, and temperature distribution is not taken into account.

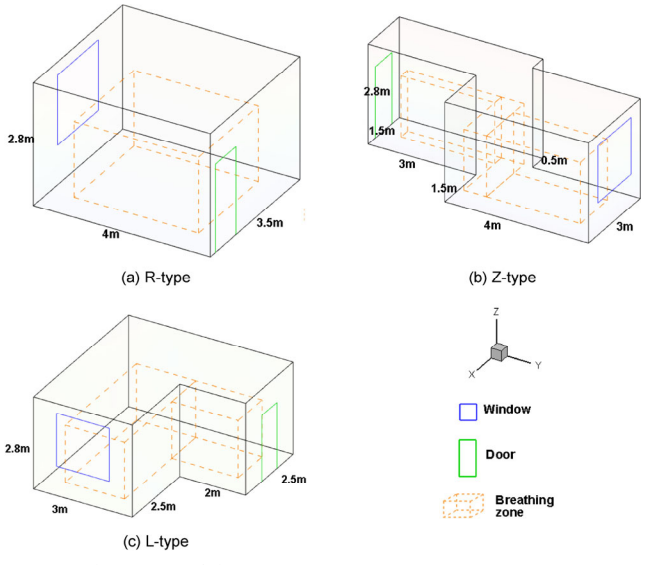

Fig. 1 Schematics of the room types

Two natural ventilation modes were investigated. For the window-inlet mode, airflow came into the room through the window and was exhausted through the door; and for door-inlet mode, the airflow direction was opposite. For each room type and ventilation mode, six ACHs including 0.5 h^{-1}, 1 h^{-1}, 3 h^{-1}, 6 h^{-1}, 12 h^{-1} and 20 h^{-1} (Foat et al. 2017) were analysed, where ACH is calculated by dividing the volumetric flow rate (m^3/h) by the room volume (m^3). Therefore, a total of 36 airflow scenarios were simulated. Besides, Nazaroff (2004) classified particles into three size ranges: ultrafine (≤ 0.1 μm), accumulation (0.1–2 μm), and coarse (≥ 2 μm) according to different particle dynamic behaviours. Therefore, the deposition velocities for particles with diameters of 0.05 μm, 0.1 μm, 0.5 μm, 1 μm, 2.5 μm and 5 μm were calculated for each airflow scenario.

2.3 Numerical method and validation

The simulation utilized Fluent 14.0 to obtain the airflow field (ANSYS 2011). The Re-Normalization Group (RNG) k-ε model was used to solve the turbulent flow because the RNG k-ε model has a good overall performance compared to the other models in terms of accuracy, computing efficiency, and robustness (Li et al. 2018). The RNG k-ε model can be given by the following expression:

$$\rho \frac{\partial \bar{\Phi}}{\partial t} + \rho \overline{u_j} \frac{\partial \bar{\Phi}}{\partial x_j} - \frac{\partial}{\partial x_j}\left[\Gamma_{\Phi,\mathrm{eff}} \frac{\partial \bar{\Phi}}{\partial x_j} \right] = S_{\Phi} \tag{10}$$

where ρ is the air density, Φ represents variables, $\Gamma_{\Phi,\mathrm{eff}}$ is the effective diffusion coefficient, and S_{Φ} represents the source term of an equation; the specific meaning of each term can be found in the study of Zhang et al. (2007).

The SIMPLE algorithm was adopted for coupling pressure and velocity, the "PRESTO!" discretization scheme was chosen, and the second-order upwind discretization scheme was used for the rest variables. The scaled residuals were set as 0.0001 for all variables, and the enhanced wall function was selected as the wall treatment. Velocity magnitudes of several points in the room were also monitored as another criterion to confirm the convergence.

The inlet adopted the velocity inlet boundary, and the outlet adopted the pressure-out boundary. For low ACH, the mass flow rate will be overestimated if the inlet cells are all open. For solving this problem, Zhang et al. (2009) proposed a random mathematical function to determine the actual opening ratio. The function can be described as follows:

$$\text{Random}\ (i) \le \varepsilon \tag{11}$$

where Random (i) is a mathematical function to obtain a random number that changes from 0 to 1, ε is the ratio

of the opening area to the total area, and i is the CFD cell index, which increases from 1 to N. The errors between the random ACHs and the required ACHs were controlled within 5%. The turbulence kinetic energy and dissipation rate for the inlet flow can be calculated by $k_{\text{inlet}} = 1.5 \times (U \times I)^2$ and $\varepsilon_{\text{inlet}} = (k_{\text{inlet}})^{1.5} / (0.005\sqrt{A_{\text{inlet}}})$ (Bartak et al. 2001), respectively. As mentioned in Section 2.1, You et al. (2012) developed empirical equations to calculate the particle deposition velocity on different angles of smooth planar surfaces with various particle diameters. Their algorithm was solved in FLUENT through the user defined functions (UDFs) code.

Gambit 2.4.6 was used to generate hexahedral meshes for discretizing the governing equations. Meshes near the door, window and wall were refined with the Y plus value below five. Through the grid independence test, the grid mesh numbers in the R-type, Z-type, and L-type rooms were 157464, 201042 and 452540, respectively. The validation of the numerical method is reported in the Appendix, which can be found in the Electronic Supplementary Material (ESM) in the online version of this paper. The divergence between the predicted and experimental values is within the accepted range. Because the case used in the validation has the similar flow problems as this study, that is, sub-configuration validation (van Hooff et al. 2018), we thought the numerical model was also acceptable for this study.

3 Results and discussion

3.1 Mixing factor

The mixing factors under different scenarios are presented in Fig. 2. From this figure, we find that when the window is the inlet, the mixing factor is higher than that when the door is the inlet. This outcome occurs because when the door is used as the entrance of fresh air, the fresh air is mixed strongly with the indoor air, and the mixing factor is close to one. However, when the air is supplied from the window, fresh air is delivered to the breathing zone directly, the air in the breathing zone is quickly replaced by the fresh air, and the mixing factor is larger.

Because the window opening behaviour is more common, we investigated the mixing factor variation under the window-inlet mode. As shown in Fig. 2, the mixing factors present a V-shaped distribution with the ACH under the window-inlet mode. Figure 3 shows the velocity fields of the R-type room for different ACHs (1 ACH, 6 ACHs, 20 ACHs) under the window-inlet mode. For the scenario with an ACH of 1 (Fig. 3(a)), the flow pattern is close to "stratum ventilation"; most of the fresh air is delivered to the breathing zone, and the velocity gradient in the breathing

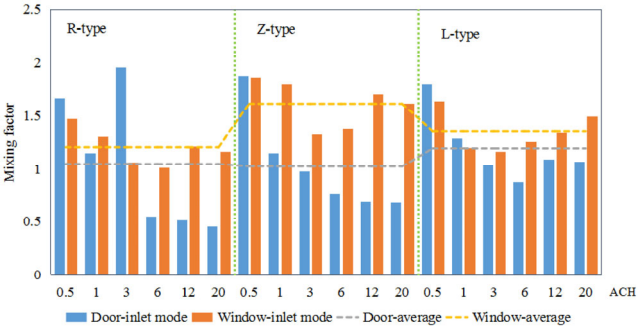

Fig. 2 Mixing factors for different scenarios

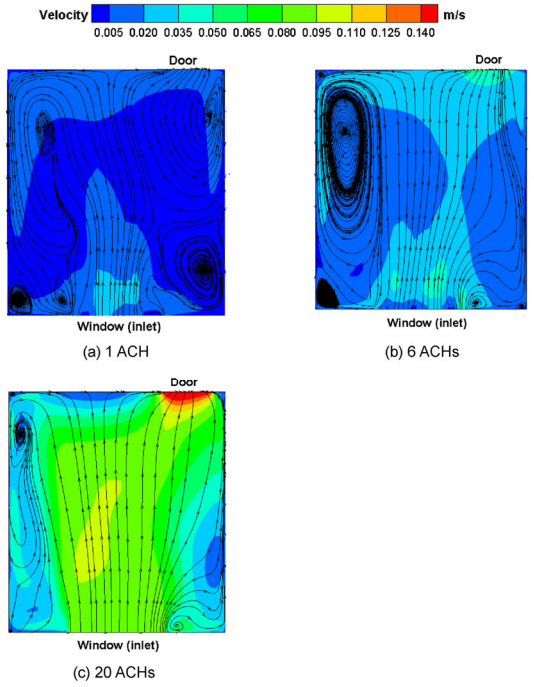

Fig. 3 Velocity fields for the R-type room under the window-inlet mode (z=1.2 m)

zone is obvious along the direction of the airflow. Therefore, its mixing with the indoor air is weak which results in a higher mixing factor. The condition is similar when the ACH is 20 (Fig. 3(c)), for which the flow pattern appears to be "piston ventilation", and the airflow velocity is much larger. However, when the ventilation rate is 6 ACHs (Fig. 3(b)), the mixing of the fresh air and indoor air is strong due to the airflow vortex, and this leads to a lower mixing factor.

For the effect of room type, the Z-type room has the largest mixing factor, and the R-type room has the smallest mixing factor, while the average mixing factors of the R-type, Z-type and L-type were 1.13, 1.32 and 1.27, respectively. Although both the relative locations of the door and window of Z-type rooms and R-type rooms are close to a straight line, the shape of the Z-type room is more conducive to the formation of cross ventilation. When the ratio of the room depth and room height is between 2.5 and 5, it is easiest to

form the cross ventilation which can deliver the fresh air to the breathing zone directly. The interior space of the Z-type room is narrow, and the ratio of the room depth and room height is 2.5, while the ratio of the R-type room is only 1.43.

To explain this outcome more clearly, we introduced the Okubo-Weiss parameter, W, to analyse the mixing degree in these rooms. The Okubo-Weiss (Li et al. 2016) parameter represents the difference of deformation and vorticity square, which can be calculated by:

$$W = s_n^2 + s_s^2 - \omega^2 \tag{12}$$

where

$$s_n = \frac{\partial u}{\partial x} - \frac{\partial v}{\partial y} \tag{13}$$

$$s_s = \frac{\partial v}{\partial x} + \frac{\partial u}{\partial y} \tag{14}$$

$$\omega = \frac{\partial v}{\partial x} - \frac{\partial u}{\partial y} \tag{15}$$

where s_n is the stretching deformation, s_s is the shearing deformation, and ω is the vorticity. When the value of W is larger than 0, the airflow field is dominated by the deformation structure; otherwise, vorticity is the dominant structure. More vorticity structures mean a better mixing degree between different regions. Figure 4 shows the velocity fields and vortex structures of three rooms at 6 ACHs. From Fig. 4(a) and Fig. 4(c), the R-type room and the L-type room have large airflow vortexes. Corresponding to this, W values in Fig. 4(b) and Fig. 4(d) show the vortex structure distributions for the R-type and L-type rooms. It was found that W values for some positions on the boundary of their breathing zones were negative, which means the vorticity existed on the boundary, and the air exchange between the breathing zone and other parts was strong. However, for the Z-type room, Fig. 4(e) shows the airflow vortexes are small. Additionally, from Fig. 4(f), W values on the boundary are almost positive, indicating that the vorticity is weak. This caused the flow pattern of the Z-type room to be close to cross ventilation and produced the largest mixing factor.

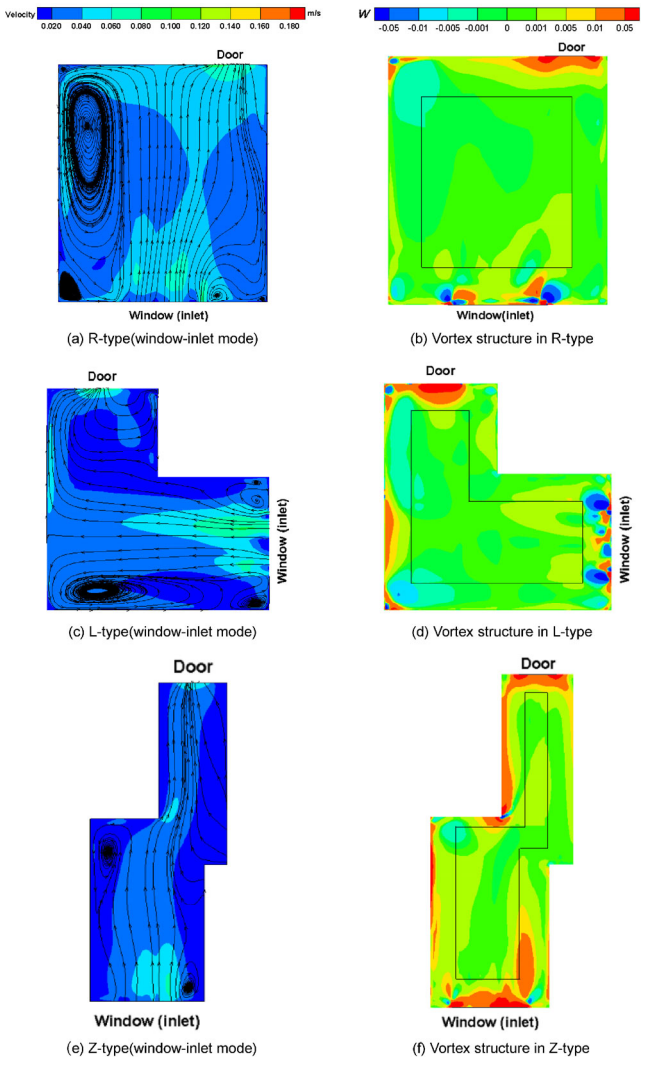

Fig. 4 Velocity fields and vortex structures for different rooms at 6 ACHs (z =1.2 m, black line: boundary of the breathing zone)

3.2 Deposition velocity

Figure 5 shows the average deposition velocities for particles with different sizes in the L-type room through Eq. (7). For scenarios under ACHs larger than three, the deposition curve as a function of particle diameters is a V-shaped curve as mentioned in a previous study (Lai and Nazaroff 2000). This resulted from different deposition mechanisms for different sized particles. For particles with a size smaller than 0.1 μm, the particle deposition is dominated by turbulence

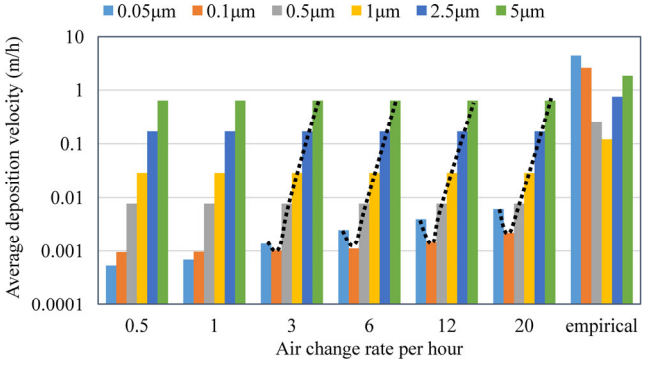

Fig. 5 Average particle deposition velocities for the L-type room

and the Brown diffusion, while for particles larger than 0.1 μm, gravitational sedimentation is the dominant factor. The total effect of diffusion and gravity for particles with diameter of 0.1 μm was minimal; therefore, the average deposition velocity is relatively smaller.

It is also indicated that the ACHs have little effect on the deposition velocities of particles larger than 0.1 μm but have a great influence on the deposition velocities of particles smaller than 0.1 μm, which agrees with other studies (Zhao et al. 2008; Gao and Niu 2007). And the field sampling data in the study of Liu et al. (2018) also indicated that higher natural ventilation rate would result in higher deposition velocity for PM2.5. This is because the turbulence and Brown diffusion for small particles are directly affected by the friction velocity of the wall surface (You et al. 2012). Zhao and Wu (2007) defined the friction velocity as the square root of the wall shear stress over air density, and it is determined by the near wall velocity gradient which is associated with the ACH and airflow distribution. When the ACH is smaller than three, the friction velocity near the wall surface decreases, and the deposition velocity of 0.05 μm particles decrease, which also makes the deposition curve not a V-shaped curve.

Figures 6 and 7 show the average particle deposition velocities for the R-type room and the Z-type room. Compared with the deposition velocity for the L-type room, for the particles with size larger than 0.5 μm, the deposition velocities were almost the same and independent of the room type. However, for the smaller particles (< 0.5 μm), the effect of the room type on the deposition velocity depended on the ACH. When the ventilation rate was small (ACH < 3), the deposition velocities of these smaller particles were

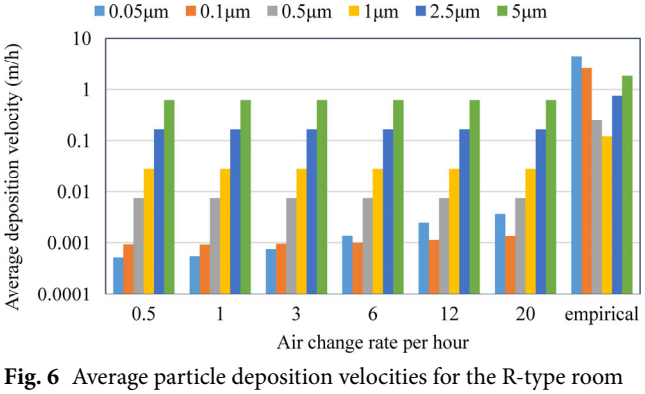

Fig. 6 Average particle deposition velocities for the R-type room

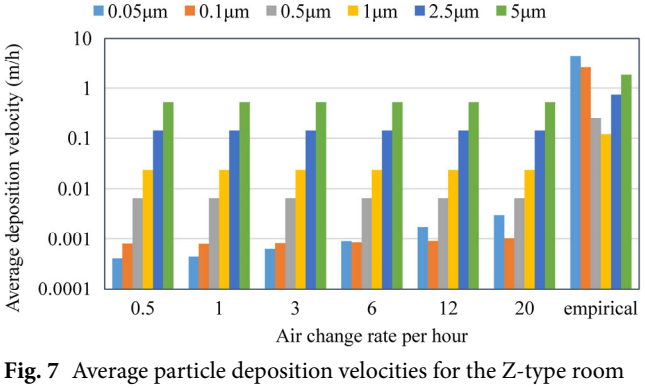

Fig. 7 Average particle deposition velocities for the Z-type room

almost the same for each room type; but when the ventilation rate increased (ACH > 3), their deposition velocities increased significantly, and the differences between different room types were obvious. The L-type room had the highest deposition velocity for particles with the size smaller than 0.5 μm. This may be because the large vortex region in the L-type room enhanced the near wall velocity gradient which resulted in a higher friction velocity on the wall surfaces.

In addition, Shi et al. (2016) summarized the experimental data and proposed an empirical equation to calculate the deposition velocity for different sized particles. The equation is as follows:

$$\overline{v_d(d_p)} = 2.89 \times (\log d_p)^2 + 0.43 \times (\log d_p) + 0.12 \quad (16)$$

We used the formula to calculate the deposition velocities for the particle sizes in this study and added the results in Figs. 5–7. As shown in the figures, the values from the empirical equation are different from those from the CFD model. This is because the empirical equation is only related to the particle diameter and does not consider other factors, such as the room type and air exchange rate. It seems an averaged deposition velocity of the experimental measurements. Therefore, in the application of the multi-zone model, it is not appropriate to use the fixed deposition velocity obtained through the empirical equation, and the influences of the room type, ACH and natural ventilation mode on the deposition velocity should be considered.

3.3 Limitations and future study

Three room types and 36 scenarios are selected for this study, and these cases include primarily common room types, ventilation rates, and particle sizes. The results of the mixing factor and deposition velocity can be used as adjustment factors in the mass balance equations of the multi-zone model. In the future, we will investigate more scenarios to cover some specific room types and conditions, and further improve the accuracy of calculating the mixing factors and deposition velocities by considering the influences of barriers and moving people (Cao et al. 2017).

In this study, the CFD tool was used to analyse the mixing factor and particle deposition velocity in this study due to its cost, time and labour-saving abilities. In the simulation, we obtained the detailed information of scenarios we studied, and the information was important to determine the cause and effect. Experimental investigations will be conducted to further validate the predicted mixing factors and particle deposition velocities for different room types, natural ventilation rates, and inlet-modes, as well as the compensation effect of these parameters for the multi-zone model.

4 Conclusions

In this study, we used numerical simulation including the RNG model and the deposition algorithm from the literature to investigate the mixing factors and particle deposition velocities for 36 cases with different room types, natural ventilation rates and inlet-modes. Based on the simulation results, conclusions can be drawn as follows:

1) The mixing factor of the Z-type room was the highest compared with other types of rooms under the same ventilation rate. The average mixing factors of the R-type, Z-type and L-type were 1.13, 1.32 and 1.27, respectively. The mixing factors presented V-shaped distributions with the change in the air exchange rate under the window-inlet mode whose mixing factor was higher than that of the door-inlet mode.

2) With the air change rate larger than three, the deposition curve as a function of particle diameters (0.05 μm, 0.1 μm, 0.5 μm, 1 μm, 2.5 μm, 5 μm) is a clear V-shaped curve. However, there is no such trend for the particles with small air change rate. The results also showed that the deposition velocity increased with the increment of air change rate, and the L-type room had the highest particle deposition velocity.

From this study, we can find that in different scenarios, the mixing factor and particle deposition velocity are different, indicating that an adjustment of these parameters is required for the multi-zone model based on the room type, ventilation mode and particle size.

Acknowledgements

This study was supported by the National Natural Science Foundation of China (No. 51708286), the Natural Science Foundation of Jiangsu Province (No. BK20171015), the National Natural Science Foundation of China (Nos. 51478468, 51508267, 51508299), the National Basic Research Program of China (973 Program, No. 2015CB058003).

Electronic Supplementary Material (ESM): supplementary material is available in the online version of this article at https://doi.org/10.1007/s12273-018-0497-x.

References

ANSYS (2011). ANSYS Fluent 14.0 User's Guide.

ASHRAE (2004). Ventilation for Acceptable Indoor Air Quality, Atlanta: American Society of Heating, Refrigerating and Air-Conditioning Engineers.

Axley J (2007). Multizone airflow modeling in buildings: History and theory. *HVAC&R Research*, 13: 907–928.

Bartak M, Cermak M, Clarke JA, Denev J, Drkal F, Lain M, Macdonald IA, Majer M, Stankov P (2001). Experimental and numerical study of local mean age of air. In: Proceedings of the 7th International IBPSA Building Simulation Conference, Rio de Janeiro, Brazll, pp. 773–779.

Brief RS (1960). Simple way to determine air contaminants. *Air Engineering*, 2: 39–41.

Cao SJ, Cen D, Zhang W, Feng Z (2017). Study on the impacts of human walking on indoor particles dispersion using momentum theory method. *Building and Environment*, 126: 195–206.

Chen Q (2009). Ventilation performance prediction for buildings: A method overview and recent applications. *Building and Environment*, 44: 848–858.

Chen C, Zhao B (2011). Review of relationship between indoor and outdoor particles: I/O ratio, infiltration factor and penetration factor. *Atmospheric Environment*, 45: 275–288.

Constance JD (1970). Mixing factor is guide to ventilation. *Power*, 114: 56–57.

Deng H-Y, Feng Z, Cao S-J (2017). Influence of air change rates on indoor CO_2 stratification in terms of Richardson number and vorticity. *Building and Environment*, 129: 74–84.

Drivas PJ, Simmonds PG, Shair FH (1972). Experimental characterization of ventilation systems in buildings. *Environmental Science and Technology*, 6: 609–614.

Foat TG, Nally J, Parker ST (2017). Investigating a selection of mixing times for transient pollutants in mechanically ventilated, isothermal rooms using automated computational fluid dynamics analysis. *Building and Environment*, 118: 313–322.

Gadgil AJ, Lobscheid C, Abadie MO, , Finlayson EU (2003). Indoor pollutant mixing time in an isothermal closed room: An investigation using CFD. *Atmospheric Environment*, 37: 5577–5586.

Gao NP, Niu JL (2007). Modeling particle dispersion and deposition in indoor environments. *Atmospheric Environment*, 41: 3862–3876.

He C, Morawska L, Gilbert D (2005). Particle deposition rates in residential houses. *Atmospheric Environment*, 39: 3891–3899.

van Hooff T, Nielsen PV, Li Y (2018). Computational fluid dynamics predictions of non-isothermal ventilation flow—How can the user factor be minimized? *Indoor Air*, 28: 866–880.

Kang T-W, Chang T-H (2005). Analysis of ventilation performance using a model chamber. *Journal of the Korean Society of Marine Engineering*, 29(7): 24–31.

Lai ACK, Nazaroff WW (2000). Modeling indoor particle deposition from turbulent flow onto smooth surfaces. *Journal of Aerosol Science*, 31: 463–476.

Lidwell OM, Lovelock JE (1946). Some methods of measuring ventilation. *Journal of Hygiene (Cambridge)*, 44: 326–332.

Li F, Liu J, Ren J, Cao X, Zhu Y (2016). Numerical investigation of airborne contaminant transport under different vortex structures in the aircraft cabin. *International Journal of Heat and Mass Transfer*, 96: 287–295.

Li F, Liu J, Ren J, Cao X (2018). Predicting contaminant dispersion using modified turbulent Schmidt numbers from different vortex structures. *Building and Environment*, 130: 120–127.

Liu C, Yang J, Ji S, Lu Y, Wu P, Chen C (2018). Influence of natural ventilation rate on indoor PM2.5 deposition. *Building and Environment*, 144: 357–364.

Lorenzetti DM, Dols WS, Persily AK, Sohn MD (2013). A stiff, variable time step transport solver for CONTAM. *Building and Environment*, 67: 260–264.

Michaelides MP, Reppa V, Christodoulou M, Panayiotou CG, Polycarpou MM (2014). Contaminant event monitoring in multi-zone buildings using the state-space method. *Building and Environment*, 71: 140–152.

Nazaroff WW (2004). Indoor particle dynamics. *Indoor Air*, 14(Suppl 7): 175–183.

Ndione J, Yoshino H, Mochida A (2008). New Method of Coupling Multizone and CFD for Building Simulation. *Journal of Asian Architecture & Building Engineering*, 7: 125–129.

Shi S, Chen C, Zhao B (2015). Air infiltration rate distributions of residences in Beijing. *Building and Environment*, 92: 528–537.

Shi S, Chen C, Zhao B (2016). Modifications of exposure to ambient particulate matter: Tackling bias in using ambient concentration as surrogate with particle infiltration factor and ambient exposure factor. *Environmental Pollution*, 94: 1024–1029.

Wang L, Chen Q (2008a). Applications of a Coupled Multizone-CFD Model to Calculate Airflow and Contaminant Dispersion in Built Environments for Emergency Management. *HVAC&R Research*, 14: 925–939.

Wang L, Chen Q (2008b). Evaluation of some assumptions used in multizone airflow network models. *Building and Environment*, 43: 1671–1677.

Wang LL, Dols WS, Chen Q (2010). Using CFD capabilities of CONTAM 3.0 for simulating airflow and contaminant transport in and around buildings. *HVAC&R Research*, 16: 749–763.

You R, Zhao B, Chen C (2012). Developing an empirical equation for modeling particle deposition velocity onto inclined surfaces in indoor environments. *Aerosol Science and Technology*, 46: 1090–1099.

Zhai Z, Jin Q (2018). Identifying decaying contaminant source location in building HVAC system using the adjoint probability method. *Building Simulation*, 11: 1029–1038.

Zhang Z, Zhang W, Zhai ZJ, Chen QY (2007). Evaluation of various turbulence models in predicting airflow and turbulence in enclosed environments by CFD: Part-2: Comparison with experimental data from literature. *HVAC&R Research*, 13: 871–886.

Zhang TT, Lee K, Chen QY (2009). A simplified approach to describe complex diffusers in displacement ventilation for CFD simulations. *Indoor Air*, 19: 255–267.

Zhao B, Wu J (2007). Particle deposition in indoor environments: analysis of influencing factors. *Journal of Hazardous Materials*, 147: 439–448.

Zhao B, Yang C, Yang X, Liu S (2008). Particle dispersion and deposition in ventilated rooms: Testing and evaluation of different Eulerian and Lagrangian models. *Building and Environment*, 43: 388–397.

Zhao B, Chen C, Tan Z (2009). Modeling of ultrafine particle dispersion in indoor environments with an improved drift flux model. *Journal of Aerosol Science*, 40: 29–43.

Zhong K (2004). Investigation on the relationships of indoor and outdoor air pollutant concentrations during the evolution process. PhD Thesis, Xi'an University of Architecture and Technology, China. (In Chinese)